Journal of Catalysis 259 (2008) 147–160

Contents lists available at ScienceDirect

Journal of Catalysis

www.elsevier.com/locate/jcat

First principles calculations and experimental insight into methane steam reforming over transition metal catalysts

Glenn Jones [a], Jon Geest Jakobsen [b,c], Signe S. Shim [b,c], Jesper Kleis [a], Martin P. Andersson [a], Jan Rossmeisl [a], Frank Abild-Pedersen [a], Thomas Bligaard [a], Stig Helveg [c], Berit Hinnemann [c], Jens R. Rostrup-Nielsen [c], Ib Chorkendorff [b], Jens Sehested [c], Jens K. Nørskov [a,*]

[a] Center for Atomic-Scale Materials Design (CAMD), Department of Physics, Building 307, Technical University of Denmark, DK-2800 Kgs. Lyngby, Denmark
[b] Center for Individual Nanoparticle Functionality (CINF), Department of Physics, Building 312, Technical University of Denmark, DK-2800 Kgs. Lyngby, Denmark
[c] Haldor Topsøe A/S, Nymøllevej 55, DK-2800 Kgs. Lyngby, Denmark

ARTICLE INFO

Article history:
Received 22 May 2008
Revised 31 July 2008
Accepted 5 August 2008
Available online 3 September 2008

Keywords:
DFT
Steam reforming
TEM
Kinetics
Reactivity trends
Noble metals
Surfaces
Nanoparticles

ABSTRACT

This paper presents a detailed analysis of the steam reforming process from first-principles calculations, supported by insight from experimental investigations. In the present work we employ recently recognised scaling relationships for adsorption energies of simple molecules adsorbed at pure metal surfaces to develop an overview of the steam reforming process catalyzed by a range of transition metal surfaces. By combining scaling relationships with thermodynamic and kinetic analysis, we show that it is possible to determine the reactivity trends of the pure metals for methane steam reforming. The reaction is found to be kinetically controlled by a methane dissociation step and a CO formation step, where the latter step is found to be dominant at lower temperatures. The particle size of the metal catalysts particles have been determined by transmission electron microscopy (TEM) and the turn over frequency observed to be linearly dependent on the dispersion, supporting the theoretical notion that the active sites are most likely present as one dimensional edges. It has been found that determination of the correct particle size distribution of small (2–4 nm) Ru particles requires *in situ* TEM measurements under a hydrogen atmosphere. The overall agreement between theory and experiment (at 773 K, 1 bar pressure and 10% conversion) is found to be excellent with Ru and Rh being the most active pure transition metals for methane steam reforming, while Ni, Ir, Pt, and Pd are significantly less active at similar dispersion.

1. Introduction

Our dependence on fossil fuels can be found in areas such as energy production and manufacture of nearly all man-made bulk chemicals. In spite of the necessity to move towards bio- and renewable chemical sources in the future [1–3], the importance of large fossil fuel based industrial processes cannot be over-emphasized and will remain central for a number of years to come. The need for cleaner and more efficient catalysis technologies is therefore greater than ever. Steam reforming is an industrial process of key importance. Natural gas and other liquid hydrocarbons are converted into synthesis gas or hydrogen which can subsequently be transformed to higher value chemicals. The process is a first step in converting natural gas resources to valuable products like petroleum, diesel, methanol, and ammonia. Moreover, steam reforming processes can act as a source of hydrogen and are therefore potentially important in any emerging hydrogen economy. A detailed review of this reforming process and its applications can be found in reference [4].

Steam reforming is traditionally performed over Ni-based catalysts [4] in tubular reformers with the catalyst placed inside 10–12 m long tubes situated in a fired oven. The temperatures vary from 450 °C at the inlet up to 950 °C at the outlet. The effectiveness factor of the catalyst is high (1–0.2) at the inlet but falls below 0.1 after 2 m from the inlet when reaching approximately 600 °C [5]. Noble metals such as Ru [6,7], Rh [7,8], Pd [7], Ir [7,9,10], and Pt [7,11] are also active for steam reforming but these metals are normally too expensive to be used in conventional industrial reformers.

There have been a number of studies that have addressed the order of reactivity between the different transition metals. Rostrup-Nielsen [12] and Kikuchi et al. [13] performed some of the first detailed studies of steam reforming over transition metal catalysts in the early nineteen-seventies. Rostrup-Nielsen [12], measured the rate of steam reforming of ethane at atmospheric pressure and 773 K, which correlated directly with the rate of steam reforming of methane. The relative activity was found to be:

Rh, Ru > Ni, Pd, Pt > Re > $Ni_{0.7}Cu_{1.3}$ > Co.

* Corresponding author. Fax: +45 45253175.
E-mail address: norskov@fysik.dtu.dk (J.K. Nørskov).

0021-9517/$ – see front matter
doi:10.1016/j.jcat.2008.08.003

Kikuchi et al. [13] studied steam reforming of methane at atmospheric pressure in the temperature range 623–873 K and observed a similar sequence of the relative activity between the group VIII metals,

Rh–Ru > Ni > Ir > Pd ∼ Pt ≫ Co, Fe.

Kikuchi et al. [13] proposed that the kinetics should follow dependencies on methane and water as $r = k(P_{CH_4})^0(P_{H_2O})^{0.5}$, arguing that there should be no methane dependency of the rate on Ru and Rh pure metals. This kinetic expression is not in agreement with the most recent published activity measurements by Wei and Iglesia as discussed below.

Rostrup-Nielsen and Hansen [7] conducted a series of experiments with Ru, Rh, Pd, Ir, Ni and Pt on MgO supports, measuring steam reforming activity at 823 K and atmospheric pressure. The relative activities were reported to be:

Ru, Rh > Ir > Ni > Pt, Pd.

Qin et al. [14] performed similar experiments as Rostrup-Nielsen et al. [7] with noble metals on a MgO support and found an almost identical activity relationship for the noble metal catalysts as the two previous mentioned studies under reaction conditions with a temperature range of 873–1173 K and atmospheric pressure:

Ru > Rh > Ir > Pt > Pd.

It should be noted that support effects were shown to be minimal, with Pd, Pt and Rh on Ceria having a similarly high rate compared to a silicate support [15].

It thus appears that there is a reasonably general consensus regarding the trend in the order of reactivity. Of the pure metal catalysts Ru and Rh are the most active, Ni and Ir are intermediate and Pd and Pt are less active. However, Wei and Iglesia [6,8–11,16] have recently made carefully designed kinetic investigations of a series of metal catalysts for methane steam reforming. It was surprisingly found for the metals investigated (Ru [6], Rh [8], Pt [11], Ir [9,10], and Ni [16]) that the relative activity order was:

Pt > Ir > Rh > Ru, Ni.

Interestingly, Wei and Iglesia found that Pt is the most active and that Ir is also more active than Rh and Ru. Wei and Iglesia also showed that the turnover frequency increases with increasing dispersion indicating that the detailed metal nanoparticle structure must play a role for the activity—an observation that could be important for the comparison with previous work. Furthermore Harrison et al. [17] have highlighted a discrepancy in the measured sticking coefficient for single crystal Ru [18], this will be subject to discussion later in the paper.

The kinetics of the steam reforming reaction has been the subject of numerous interpretations and discussions as illustrated lately [16]. The thorough investigations by Wei and Iglesia showed that dissociation of methane is the rate-determining step for both steam and CO_2 reforming of methane. This mechanism was verified at 873 K and various pressures for a range of metals (Ni, Ru, Pt, Rh, and Ir) [16]. It has been shown by other authors that for different transition metals there was a difference between steam and CO_2 reforming reactivity, attributing this to blocking of the active sites by CO [7]. There is a general trend in previous studies, showing that the reaction kinetics are first-order with respect to methane. However, different studies invoke various parameters to be included in the kinetic expression in order to readily explain other phenomena, such as the H_2O dependency [19] or pressure dependency [2]. Therefore, it may be that the activity is not governed by a single rate determining step, but several rate determining steps depending on the reaction conditions [4].

This paper will present a detailed analysis of the methane steam reforming process from first-principles calculations, and compare the results with experimental investigations of the reactivity of supported nanoparticles. Several groups have published results from calculations for CH_4 activation [20–39], however these have not dealt with the full catalytic process of steam reforming under industrial conditions. In the present work we employ recently recognised scaling relationships for adsorption energies (of hydrogenated atoms) adsorbed at pure metal surfaces, to develop an overview of the trends underlying the steam reforming process catalyzed by transition metals. These relationships allow total energies of reaction intermediates to be estimated and used in a complementary fashion alongside detailed density functional theory calculations. Once the detailed energetics are established, thermodynamic analysis can be applied to the total energies in order to account for temperature and pressure effects. The approach is particularly important because the entropic effects become significant at the high reaction temperatures necessary for the steam reforming process. Finally, the thermodynamic analysis allows us to parameterize a kinetic model from which we can determine turn-over frequencies (TOF) for a range of pure metals. This opens up both the possibility of establishing a detailed understanding of the relative rates of pure metal catalysts, as well as the possibility for a future rational search for improved steam reforming alloy catalysts.

To validate and expand the theoretical model, we combine the first principles calculations with experimental investigations of the steam reforming process. The experimental work will report on the steam reforming activity for a series of catalysts (Ni, Pt, Ru, Rh, Ir, Pd), primarily supported on ZrO_2 and Al_2O_3. The activity experiments are performed at atmospheric pressure and 773 K, at conditions far from equilibrium. The activities are correlated with structural information in terms of the metal dispersions of the catalysts, which are determined from (environmental) transmission electron microscopy (TEM) and supported by sulphur chemisorption and X-ray powder diffraction (XRPD). From the dispersions and the activities it is possible to evaluate the relative turn-over frequencies (TOF) for the metal catalysts studied here. The results show a clear dependency of the steam reforming activity on different types of metals and a significant increase in the activity with increasing dispersion. The experimental determination of the TOF and the dispersion allows direct comparison and benchmarking of the theoretical results.

2. Theoretical methodology

DFT is used as implemented in the computer code DACAPO using the RPBE exchange correlation functional [40]. Previous work has shown that the important active sites for a number of catalytic processes are the steps [33,41–44]. That this is also the case for methane dissociation was also recently demonstrated for a stepped Ni(111) surface where it was possible to separate the reactivity of the steps from that of the terraces. The ratio of turn over frequencies was found to be a factor of 200, which was in good agreement with theoretical calculations [45]. Steps thus present a lower activation barrier for steam reforming than close-packed terrace sites and the results presented here have therefore been calculated on stepped surfaces. In order to establish the adsorption energetics of hydrogenated intermediates scaling relationships were combined with the relative energies from Ref. [46] for adsorption on the fcc{211} surface for the close-packed (fcc and hcp) metals and bcc{210} surface for the bcc metals.[1] Unit cells of (2×1) periodicity were used with a depth of 10 atomic layers and a vacuum

[1] Experience has shown that modelling hcp with fcc stepped surface provides a good model and captures the desired trends. However using bcc metals in an fcc

region of 10 Å. An electronic plane wave cut-off of 340 eV was used, with the Brillouin zone being sampled by a Monkhorst–Pack [47] mesh of $\{4 \times 4 \times 1\}$. Pseudopotentials of the Vanderbilt [48] type were used to describe the electronic core regions.

Linear scaling relationships were used as discussed in reference [49]. In brief, the basic theory shows that an estimate of the adsorption energy of a given species is obtained from a linear relationship having a slope given by the valency parameter γ. If we have calculated the energy of all reaction intermediates, $\Delta E_{M1}^{AH_x}$, for one metal, M1, we can therefore estimate the energy, $\Delta E_{M2}^{AH_x}$, of the same intermediate on another metal, M2, from the adsorption energies of atom A on the two metals as:

$$\Delta E_{M2}^{AH_x} = \Delta E_{M1}^{AH_x} + \gamma(x)\left(\Delta E_{M2}^{A} - \Delta E_{M1}^{A}\right), \tag{1}$$

where γ is given by $(x_{max} - x)/x_{max}$, where x_{max} is the number of hydrogen atoms required to provide sufficient electrons to fulfill the octet rule of a given atomic species and x is the number of hydrogen atoms in the species for which the adsorption energy is determined.

This approach allows us to screen a wide range of metals [50], achievable through the knowledge of either the adsorption energy of the parent atom in question and the knowledge of all the species on a single metal. This paper has used values calculated from full DFT calculations carried out on Ru $\{10\bar{1}5\}$ surfaces for M1, and used a database of adsorption energies [46] to obtain the values for M2.

Two further relationships are necessary to fully parameterise the adsorption energies required for the steam reforming process. They relate the adsorption energy of CO to C and also the adsorption of H to C. For the purposes of this paper they are presented in a phenomenological fashion and further details, along with the calculated DFT energies can be found in the supporting material.

In order to determine scaled values for the transition state, it is also possible to use linear energy relationships determined from DFT calculations. An example of such a class is the so-called Brønsted–Evans–Polanyi relationship (BEP) [51]. The transition state barrier for a process is plotted against ΔE of the elementary step or another suitable descriptor. It is often found that a linear scaling does exist and the dependence on the barrier height to the descriptor can thus be obtained. This approach has been used to determine an expression for the CO formation step [52]:

$$\Delta E_{C^*+O^*\rightarrow CO^*}^{Act.} = \alpha \Delta E_{CO^*-C^*-O^*} + \beta, \tag{2}$$

where $\Delta E_{C^*+O^*\rightarrow CO^*}^{Act.}$ is the activation barrier for CO formation, $\Delta E_{CO^*-C^*-O^*}$ is the energy of reaction for the formation of adsorbed CO from adsorbed C and O, α and β are parameters from the straight-line fit. The relationship determining the CH_4 dissociation barrier is derived from the BEP relationship between the activation barrier for CH_4 dissociation, $\Delta E_{CH_4(g)\rightarrow CH_3^*+H^*}^{Act.}$, and the energy of reaction for the dissociative adsorption of CH_4, $\Delta E_{CH_3^*-H^*-CH_4(g)}$:

$$\Delta E_{CH_4(g)\rightarrow CH_3^*+H^*}^{Act.} = \alpha \Delta E_{CH_3^*-H^*-CH_4(g)} + \beta. \tag{3}$$

The equation is based on a linear relationship between the adsorption energy of C and the adsorption energies of both CH_3 and H and that the energy of $CH_4(g)$ is constant. By plotting the barrier height for CH_4 dissociation against the adsorption energy of C we obtain a linear relationship, which to a first approximation gives us the activation barrier for a particular metal. The supporting information should be consulted for diagrams and tables describing these relationships.

structure is often more problematic, hence the need to model them explicitly with a bcc surface.

Thermodynamic analysis can be carried out using the total energies (E) obtained from either full DFT or scaling methods as input. In this study free energies have been calculated by employing standard formulas from statistical thermodynamics [53]. For the gas-phase species (X) at temperature (T) and pressure (P), the Gibbs free energy ($G_X^{P,T}$) is given by:

$$G_X^{P,T} = E_X + E_{ZPE} + \Delta H^{0,T} - TS^T + k_B T \ln(P/P^0), \tag{4}$$

where E_{ZPE} is the zero point energy, $\Delta H^{0,T}$ is the enthalpy change due to increasing the temperature from 0 K to T, S^T is the entropy at T, k_B is Boltzmann's constant and P^0 is standard pressure (taken to be 1 bar). The equation for calculating the energy of the adsorbed species (X′) on metal (M), $E_{X'}$, is given by: $E_{MX'} - E_M$. There is no pressure term and the enthalpy change is replaced by the change in internal energy. This leads to the following expression for ($G_{X'}^{P,T}$):

$$G_{X'}^{P,T} = E_{X'} + E_{ZPE} + \Delta U^{0,T} - TS^T. \tag{5}$$

The vibrational frequencies used within this work to determine E_{ZPE}, $\Delta U^{0,T}$ and S^T are calculated within the harmonic approximation (n.b. configurational entropy is not included). There are clearly issues regarding the validity of this approximation, particularly to the low frequency modes of surface species and internal molecular rotation around bonds. However, there is at present no simple alternative method. Given that we are considering temperatures on the order of 1000 K it is believed that a larger source of error would result from leaving the contributions out. Furthermore, only one set of vibrational calculations was carried out, on the Ru$\{10\bar{1}5\}$ surface, the values obtained were then used for the other metals. This was done primarily because carrying out the vibrational frequencies on every metal would be computationally expensive, and secondly in the spirit of utilizing the scaling relationships in order to reduce the computational cost; it would require full DFT calculations of every species on every surface to obtain all of the vibrational frequencies. Again there is undoubtedly some error introduced from this approximation, but it will still enable the essential aspects of the temperature dependency to be captured, and the variations in entropic contributions over the different surfaces are likely to be significantly smaller than the variations in adsorption energetics [54].

Once the thermodynamic quantities are determined, we are in a position to construct the kinetic model. In order to do this, two important relationships are needed. The first relates the standard free energy change of an elementary reaction step, to the equilibrium constant of a reaction:

$$K_i = \exp\left(\frac{-\Delta G_i^{0,T}}{k_B T}\right), \tag{6}$$

where K_i is the equilibrium constant of elementary step i. The second relates the standard free energy of activation, $\Delta G_i^{Act.}$ (for those steps that cannot be considered at equilibrium) to the rate constant (k_i), which in transition state theory is:

$$k_i = \frac{k_B T}{h} \exp\left(\frac{-\Delta G_i^{Act.}}{k_B T}\right), \tag{7}$$

where h is Planck's constant. This expression can be evaluated for both the forward and reverse reaction, along with the relevant coverages or gas-phase pressure of an elementary step in order to obtain the net rate of the particular step in question. The elementary steps considered in the steam reforming reaction will be presented with some discussion later in the paper.

Table 1
Overview of the catalysts investigated in this paper. The varying treatments are given by aging time and temperature. This gives rise to varying particle sizes and dispersions. The activity is given as a turn-over frequency (TOF)

Catalyst	Support	Aging time (h)	Aging temperature (K)	Average particle diameter (nm)	Dispersion (%)	TOF at 773 K (s^{-1})
1 wt% Rh-1	ZrO_2	–	–	2.7/2.2[a]	32.3	12.5
1 wt% Rh-2	ZrO_2	228	1103	8.4	10.6	1.8
5 wt% Rh-3	ZrO_2	–	–	4.5	21.0	7.4
5 wt% Rh-4	ZrO_2	72	1103	8.2	11.0	3.6
5 wt% Rh-5	ZrO_2	600	892	6.5	12.7	6.2
5 wt% Rh-6	ZrO_2	600	946	7.0	12.8	4.7
5 wt% Rh-7	ZrO_2	600	1067	9.8	9.5	2.5
5 wt% Rh-8	ZrO_2	600	1096	11.1	7.6	2.0
1 wt% Ir-1	ZrO_2	–	–	1.4/1.7[a]	82.2	2.3
1 wt% Ir-2	ZrO_2	228	1103	2.9	28.4	2.1
1 wt% Ru-1	ZrO_2	–	–	4.2/2.1[a]	48.1	19.9
1 wt% Ru-2	ZrO_2	228	1103	7.2	10.8	1.1
1 wt% Pt-1	ZrO_2	–	–	1.9/2.3[a]	58.4	2.5
1 wt% Pt-2	ZrO_2	228	1103	3.9	23.8	0.5
1 wt% Pd-1	Al_2O_3	–	–	21	54.1	1.3
14.8 wt% Ni-1	$MgAl_2O_4$	–	–	6.1	20.0	1.0
2.4 wt% Ni-2	Al_2O_3	–	–	2.7/2.8[a]	35.9	1.9
10 wt% Ni-3	Al_2O_3	–	–	2.6	40.5	2.0

[a] *Ex situ*/*in situ* measurements.

3. Experimental methods

3.1. Catalyst preparation and pre-treatment

A series of eighteen different catalysts were prepared for studying the methane steam reforming reaction over noble metal catalysts. Three different support materials were used in the preparation, an yttrium (3 mol%) stabilised ZrO_2 support, a θ-Al_2O_3 support and a $MgAl_2O_4$ spinel support with BET areas of 16, 116 and 18 m^2/g, respectively.

The metals (Ru, Rh, Ir, Pt, Ni and Pd) were impregnated by the incipient wetness method using aqueous solutions of $Ru(NO)(NO_3)_3$, $Rh(NO_3)_3$, $IrCl_3{\cdot}4H_2O$, $Pt(NH_3)_4(NO_3)_2$, $Ni(HCOO)_2$, $Ni(NO_3)_2$ and $Pd(NH_3)_4(HCO_3)_2$. 1 wt% metal catalysts and 5 wt% Rh catalysts were prepared using the ZrO_2 carrier. On the Al_2O_3 support, three samples (2.4 wt% Ni, 10 wt% Ni and 1 wt% Pd) were made. Finally, a 14.8 wt% Ni sample was prepared by impregnation on the $MgAl_2O_4$ support. All the eighteen catalysts were subsequently heated to 723 K in air followed by reduction in pure hydrogen at 1 bar and 798 K according to [4,55].

To obtain varying particle sizes, six 5 wt% Rh/ZrO_2 catalysts were aged for up to 600 h at different temperatures between 873 and 1103 K in H_2O/H_2 mixtures ($H_2O{:}H_2 = 1{:}1$) at 31 bar total pressure. Samples of 1 wt% Rh/ZrO_2, 1 wt% Ir/ZrO_2, 1 wt% Ru/ZrO_2 and 1 wt% Pt/ZrO_2 were aged at 1103 K for 228 h in a similar gas mixture. The ageing procedures rendered a total of 18 catalysts, which are listed in Table 1.

After reduction or ageing treatments, all catalysts were exposed to N_2 while cooling to room temperature and passivated at room temperature by exposure to a flow of 1% air for several hours before exposure to air. After this passivation procedure the catalysts were removed from the reactor and transferred in ambient environment to the different characterization setups.

3.2. Activity measurements

The rates of steam reforming of the catalysts were measured using a fixed bed steel reactor with an internal diameter of 7.1 mm and a thermo well with a diameter of 1.8 mm mounted inside the reactor. 10–120 mg of each catalyst was crushed to a sieve fraction of 0.3–0.5 mm and mixed with catalytically inert $MgAl_2O_4$ with the same grain size to obtain a total mass of 300 mg. The mixture of catalyst and inert material was placed in the reactor on wads of quartz wool supported on a metal plate with holes. The resulting bed height was approximately 11–12 mm. After insertion, the catalysts were first re-reduced in H_2 at 1 bar and 623 K. Subsequently the rate of methane steam reforming was measured at 773 K using a gas mixture of 19% CH_4, 7% H_2 and 74% H_2O at a total flow of 21.6 Nl/h and ambient pressure. At the reactor outlet, steam was condensed and the composition of the dry gas was analysed by a gas chromatograph (GC). The conversion was calculated from the GC analysis and the rate of methane consumption in the reactor was determined based on the methane inlet flow. The overall conversion in the reactor was used to calculate the local rate of reforming at the top of the catalyst bed by assuming that the rate (r) is described by the following expression for reforming:

$$r = k(T)p(\mathrm{CH_4}) \tag{8}$$

in accordance with the results recently obtained by Wei and Iglesia [16]. In contrast to Wei and Iglesia, we have performed kinetic studies mainly around >723–823 K which represents typical temperatures at the inlet of tubular reformers and in pre-reformers [19]. At the higher temperatures used by Wei and Iglesia, the reaction gas will be close to equilibrium in a tubular reformer with the axial temperature gradient as the main driving force for the reaction [19]. The conversions were always small (<15%) and no corrections were therefore needed to account for the finite approach to equilibrium.

3.3. Transmission electron microscopy

All catalysts were investigated by means of transmission electron microscopy (TEM) in order to determine the particle size distributions (PSDs), an average metal particle diameter, and the metal dispersion. Measurements were done *ex situ* using a Philips CM200 FEG and a Philips CM300 FEG electron microscope. For *ex situ* microscopy, a TEM specimen was prepared of each catalyst under ambient conditions by crushing the passivated catalyst to a fine powder and dispersing the powder on Cu grid covered with a holey carbon film. TEM images were recorded using a $1k \times 1k$ CCD camera at different magnifications corresponding to an image pixel size in the range of 0.08 nm to 0.45 nm. In order to enhance image contrast of the metal nanoparticles, an objective aperture was employed with a cut-off at 0.20 nm (CM200) or 0.24 nm (CM300).

Experiments were also performed *in situ* using environmental TEM (ETEM) in order to explore whether passivation affects the metal particle size. The ETEM experiments were done using a Philips CM300 FEG electron microscope equipped with an environmental cell [56]. In the ETEM experiments, the catalyst powders were distributed on a Mo TEM grid and exposed to 2.0 mbar H_2 at 773 K for about 1 h to re-reduce the catalyst. Subsequently, images were recorded *in situ* with the catalyst exposed to 1.2–1.6 mbar H_2 at 773 K. TEM images were recorded using a $1k \times 1k$ CCD at a magnification corresponding to an image pixel size of 0.12 nm. An objective aperture was employed with a cut-off at 0.26 nm.

From the TEM or ETEM images, the metal nanoparticle diameters are determined from the projected area of the particles assuming that the particles are spherical. The resulting particle size distributions allow surface-averaged diameters to be compared to sulphur chemisorption experiments and volume-averaged particle diameters to be compared to the average particle diameters ob-

tained by XRD methods.[2] The surface-averaged particle diameter is given by

$$d_s = \frac{\sum n_i d_i^3}{\sum n_i d_i^2}$$

where n_i is the number of particles with diameter d_i. Likewise, the volume-averaged particle diameters are given by

$$d_v = \frac{\sum n_i d_i^4}{\sum n_i d_i^3}.$$

The dispersion can then be determined from the total surface area (A_{tot}) and the total volume (V_{tot}) determined from the particle size distributions by the following equation:

$$D = \frac{A_{tot}}{V_{tot}} \cdot \frac{v}{s} = 6 \cdot \frac{\sum n_i d_i^2}{\sum n_i d_i^3} \cdot \frac{v}{s}, \quad (9)$$

where v is the atomic volume and s is the surface area per atom. If we assume that the close-packed surfaces which have the lowest surface energies are dominant, then it is possible to calculate the dispersion for an fcc(111) metal particle by

$$D = \frac{\sum n_i d_i^2}{\sum n_i d_i^3} \cdot \frac{6a}{\sqrt{3}}$$

and for an hcp(0001) metal particle by

$$D = \frac{\sum n_i d_i^2}{\sum n_i d_i^3} \cdot 3 \cdot c,$$

with a and c being the lattice parameters.

3.4. X-ray powder diffraction

The 5 wt% Rh samples were analysed by X-ray powder diffraction (XRPD) to determine the average rhodium crystallite sizes of selected samples. It should be noted that crystallite sizes obtained by XRD are volume averaged. The XRD measurements were performed on a Philips X'Pert Pro θ–θ diffractometer with Bragg–Bretano geometry, a variable divergence slit and a graphite monochromator using Cu$K\alpha$ radiation. Average metal crystallite sizes were obtained from the line broadenings of the Rh(200) diffraction line, corrected for the instrumental broadening, using the Scherrer equation.

3.5. Sulphur chemisorption

Sulphur chemisorption was used for estimating the diameter of the metal crystals of the zirconia supported Rh catalyst according to [16,19]. As there are no systematic studies published on the H_2S/Rh system, the use of the correlation for metal crystal size and sulphur uptake as for nickel [19] represents a simplification. In brief, the catalysts were exposed to a H_2S/H_2 gas mixture until saturation. After sulphidation, the sulphur uptakes of the catalysts, in μg sulphur per gram catalyst (ppm), were determined by oxidation of the chemisorbed sulphur at high temperature and measuring the amount of generated SO_2 by means of infrared detection. The sulphur chemisorption capacity (s_{cap}) was used to estimate the dispersions and surface-averaged metal particle diameters. For nickel catalysts it is possible to correlate the sulphur chemisorption and the diameter [19]. However, for Rh catalysts the conversion of the sulphur uptake to a metal area, a surface-averaged metal-diameter and a metal dispersion is less well studied. The maximum coverage of sulphur at nickel is approximately 0.5 and this value is also assumed to be the maximum coverage of sulphur on Rh. The total number of metal surface atoms per weight, $N_{surface}$, may then be calculated from the sulphur capacity, $s_{cap.}$ (wt. ppm), the molar mass of sulphur, M_s (g/mol), the coverage of sulphur, θ_s, and Avogadros number N_A

$$N_{surface} = N_A \frac{s_{cap}}{M_s \theta_s} 10^{-6}. \quad (10)$$

The total number of Rh atoms in the catalyst can then be calculated from the weight percentage of the metal, X, and the molar mass of the Rh, M_x (g/mol)

$$N_{total} = N_A \frac{X}{M_x \cdot 100}. \quad (11)$$

Combining Eq. (10) and Eq. (11) it is then possible to estimate the dispersion of the metal based on a measurement of the sulphur capacity

$$D = \frac{1}{\theta_s} \frac{M_x}{M_s} \frac{s_{cap}}{X} 10^{-4}. \quad (12)$$

For Rh (fcc metal) is possible to estimate the average particle diameter based on the dispersion by combining Eq. (12) and Eq. (9)

$$d = \theta_s \frac{M_s}{M_x} \frac{X}{s_{cap}} \frac{6v}{s} 10^4, \quad (13)$$

where v and s are the volume and surface area of the metal x in the catalyst as given previously assuming closed packed surfaces.

4. Theoretical results

The theoretical part of the paper will develop the picture of steam reforming in a sequential manner. Starting from the simple energetic picture, we then build up the complexity by introducing reaction conditions such as pressure and temperature through thermodynamic considerations, and finally we turn the theoretical picture into a micro kinetic model of the steam reforming process. The discussion will unfold primarily to address what key parameters are important for the reaction and to establish a consistent picture of the reaction.

4.1. Thermodynamic analysis

We shall begin by considering what can be learnt by applying the scaling relationships to the construction of an energy diagram for steam reforming. Fig. 1 illustrates the overall energy diagram that can thus be constructed. Even this most simple diagram is extremely instructive, for a number of reasons. This allows one to momentarily take a step back from the intricate details, and to observe the overall trends in steam reforming reactivity of the pure metals. It is immediately observed that the noble metals Au, Ag and Cu are completely unsuitable for steam reforming with the reaction steps from $CH_4(g) + H_2O(g)$ all the way to $C^* + O^*$ being significantly uphill energetically. We can also consider the other extreme where W binds C^* and O^* so strongly that they are unlikely to react off easily, and in fact W is found to be oxidised under these conditions. In Fig. 1 a region of metals can be discerned, bounded by Pt and Ru, for which the reaction looks reasonably favourable.

When one considers the overall reaction, it can be seen that the reaction from left (reactants) to right (products) is uphill (endothermic) and it can also be observed from the stoichiometry of the reaction that the entropy is increasing (four product molecules

[2] There is not any particular merit to one or the other technique, but one needs to be aware of the subtle difference in the information obtained, due to the nature of the technique.

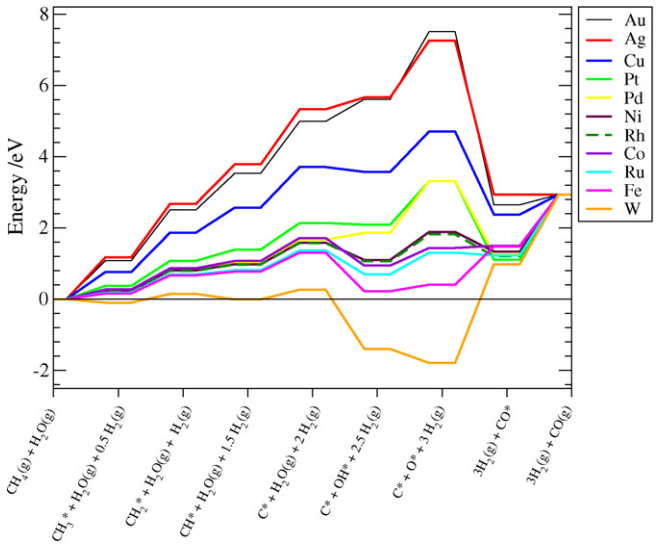

Fig. 1. The potential energy diagram for steam reforming, as determined from the linear scaling relationships. Here a range of metals from noble to highly reactive are considered.

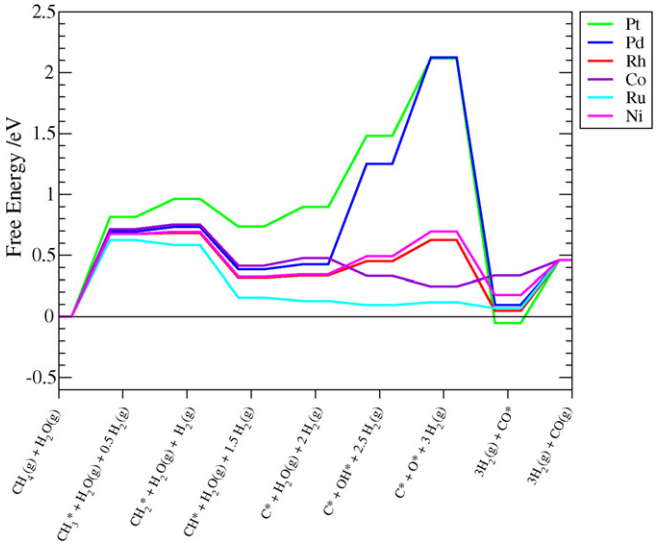

Fig. 2. Standard free energy reaction scheme for steam reforming at 773 K. The noble metals Cu, Ag and Au are now removed from consideration as are the metals that are to reactive and known to form oxides under the reaction conditions. DFT was used to calculate the energies of C*, O* and the gas phase species (as well as the Ru data which all other data was referenced to). Scaling relationships were used to determine the energies of the hydrogenated species. The data are calculated using scaling relationships to determine total energies of hydrogenated species and DFT of those remaining.

per two reactant molecules). This second point is particularly important because it implies that the $T\Delta S^T$ in the expression for the gas-phase free energy will become increasingly significant as the temperature increases. It is therefore essential to run the reaction at high temperature in order to obtain a significant conversion. Furthermore, it is important to consider the energetics under these elevated temperatures in order to simulate some of the subtleties that arise.

For clarity of discussion the focus will now be on the subset of most relevant metals, namely those in Fig. 1 that are bounded by Pt and Ru (i.e. Pt, Pd, Ni, Rh, Co, Ru). For these the thermodynamic terms at specific temperatures are now included for the purpose of calculating $\Delta G^{0,T}$. In order to facilitate the subsequent discussion, a temperature of 773 K will be used for the main body of the text. This is because the presented experimental work has been carried out at this temperature. In the supporting material graphs are included that correspond to higher temperatures (1000 K) as well as conditions which match those used in the work of Wei and Iglesia (873 K). Fig. 2 shows the reaction free energy profile at 773 K. It is observed that the overall standard free energy is increasing by a little less than 0.5 eV. It should be noted that we do not achieve a negative change in free energy at standard pressure for the reaction until ~900 K (however if we apply 1 bar of pressure and 10% conversion at 773 K we do in fact drive the final state down to the level of the initial state, implying that equilibrium at 773 K gives 10% conversion). What is clearly evident under these conditions is that Pt and Pd are very unfavourable for the adsorption and dissociation of molecular water. Furthermore, we can see that the entropy loss for the dissociative adsorption of molecular CH_4 has driven up the free energy level for this step, suggesting that this step could be rate determining under certain conditions.

We now turn our attention to Fig. 3 which is constructed using data at the same temperature as Fig. 2, but this time with the pressure contributions included, allowing us to get a different perspective. Fig. 3 illustrates the relative $\Delta G^{1,773}$ of each important surface intermediate, where rather than just examining the standard free energies we see the influence of varying the pressure upon the surface stability of each species. The conversion of methane is set at 10% and CO, CO_2, H_2 and H_2O are assumed to be equilibrated in the water gas shift reaction. The partial pressures for these four gasses are used to determine $\Delta G^{1,773}$ for each

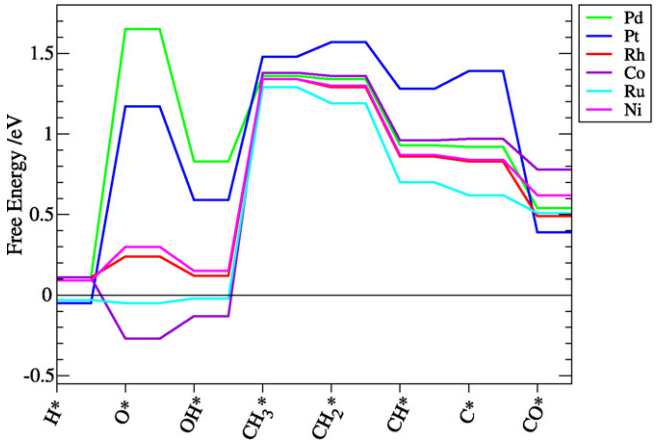

Fig. 3. Free energies of the most important surface species involved in steam reforming, referenced to CO(g), H_2O(g) and H_2(g) for steam reforming at 773 K, 10% conversion at 1 bar total pressure and assuming that the shift reaction is equilibrated. The data are calculated using scaling relationships to determine total energies of hydrogenated species, and DFT of those remaining.

surface species. Details are given in the supplementary material. Through this we can get an understanding of which species are likely to be present on the surface, and if indeed we would expect any poisoning effects. Co adsorbs O and OH more strongly than any of the other metals under consideration and it is therefore highly likely to be O poisoned (Ru is the only other metal, which has O and OH species at a negative free energy). Apart from these species it can be seen that we would expect the surface to be very clean under steam reforming conditions.

4.2. Analysis of reaction barriers

The important metals for steam reforming catalysis have now been identified and the thermochemistry of the reaction intermediates has been established. The next step is to consider the reaction barriers. In order to do this we shall first look at the

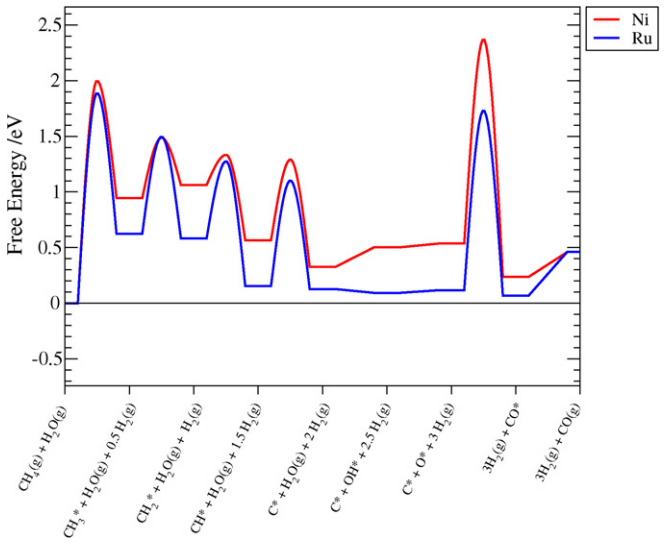

Fig. 4. Reaction free energy scheme including reaction barriers for steam reforming over stepped Ru and Ni. The plot has been constructed using DFT calculations and normal-mode analysis for the total free energies at 773 K.

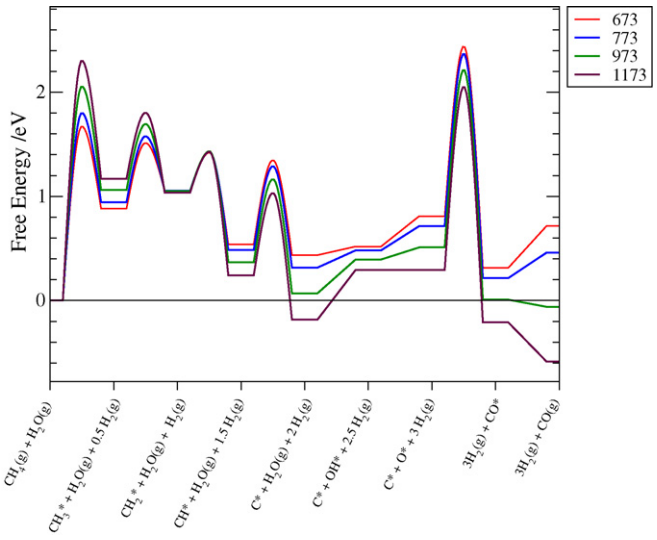

Fig. 5. Reaction scheme illustrating the temperature dependence of the steam reforming reaction over Ni at standard conditions, determined from DFT total energies.

DFT results for Ni and Ru. Ni is the metal of choice for the industrial process at present, primarily because of its abundance and therefore relatively low cost. Ru, as we have illustrated from the thermodynamic considerations, is likely to be a good candidate for the process as well, though significantly more expensive. Fig. 4 depicts the free energy diagram for Ni and Ru, along with the barriers for each hydrogenation step and the CO formation. A quick glance suggests that having a single rate determining step may be an over-simplification. In fact what what is seen is that for Ni the CO formation step looks difficult, however, on Ru there is very little to separate the CH_4 adsorption and the CO formation step.[3]

In order to answer the question of which step is the kinetically most important, we first consider the mechanism by which CO recombines. It was recently shown for methanation over Ni that at high coverages of CO (close to saturation of the preferred step site) that a dissociation mechanism involving a hydrogen atom was favoured [57]. This mechanism required the formation of a COH intermediate that then dissociated into C and OH. We might expect by time reversal that the reverse of this mechanism would hold for steam reforming. However, under steam reforming conditions we have a low CO coverage (Fig. 3). At these coverages the direct dissociation/association transition state is found to be the more stable pathway. For the CH_4 dissociation we have used a direct dissociation from the gas phase molecule, since this again is favoured at low coverages due to the need of an empty site in which to dissociate.

It has been shown recently by Inderwildi et al. [58,59] that on close packed surfaces a formyl pathway is favourable. In fact we find this pathway to be competitive for stepped Ru. However, in treating the general mechanistic overview for a series of metals the CO step is thought to be sufficient. Particularly in light of the fact that in the temperature ranges considered CH_4 activation dominates the Ru rate, and it is the less reactive metals (e.g., Ni) where the CO step competes. However, if one was to go to significantly lower temperatures where CH_4 did not dominate the reaction on Ru then an alternative mechanism would need to be included.

Using the thermodynamic analysis the discussion can be taken a step further and used to examine the reaction profile at different temperatures (see Fig. 5 for the plot corresponding to Ni). As the temperature increases the entropic contribution is such that it makes the barrier for CH_4 dissociation increase relative to the reactants free energy, whereas the free energy barrier for the CO formation step in fact decreases. This demonstrates clearly the importance of the reaction conditions on the rate of steam reforming, i.e. as T is increased the most important barrier switches from being CO formation to CH_4 dissociation. This can also be observed in the kinetic modelling to be discussed below.

The thermodynamics shows that under the experimental reaction conditions employed here, i.e. relative low temperatures, we might expect the CO formation step to be rate determining for most metals, but as the temperature is increased towards 1000 K one enters the regime where CH_4 dissociation is rate determining (passing through an intermediate regime where there is no single rate determining step). The conclusion that the CH_4 dissociation rate is rate-determining at higher temperatures, is in excellent agreement with the findings in the work of Wei and Iglesia, where relatively high temperatures (823–1023 K) were used.

A detailed picture of steam reforming has now been established, primarily based upon thermodynamic considerations of the stable species and the reaction barriers. The most promising metals have been found and subsequently the number of “good” metals has been narrowed down. The most stable species on the surface and the largest reaction barriers have been identified and the entropy dependence of the most important reaction steps has been established. This analysis will now be further developed and used to parameterise a microkinetic model.

4.3. Kinetic model

From the thermodynamic analysis it was seen that for the majority of metals under consideration the surface will be relatively clean. This implies that to a first approximation it is not necessary

[3] Here we should just point out that we are considering the rate determining step to be that which has the largest free energy barrier. This may be a reasonable assumption if one considers the expression for the rate constant and the fact that it depends exponentially on the size of the barrier. However, it is also important to consider coverage effects and this will be addressed in the modelling of the microkinetics.

explicitly to include lateral interactions.[4] We can write out our elementary steps for the steam-reforming process as follows:

$$CH_4(g) + 2^* \rightleftharpoons CH_3^* + H^*, \quad (ES1)^*$$

$$H_2O(g) + 2^* \rightleftharpoons OH^* + H^*, \quad (ES2)$$

$$OH^* + {}^* \rightleftharpoons O^* + H^*, \quad (ES3)$$

$$CH_3^* + {}^* \rightleftharpoons CH_2^* + H^*, \quad (ES4)$$

$$CH_2^* + {}^* \rightleftharpoons CH^* + H^*, \quad (ES5)$$

$$CH^* + {}^* \rightleftharpoons C^* + H^*, \quad (ES6)$$

$$C^* + O^* \rightleftharpoons CO^* + {}^*, \quad (ES7)^*$$

$$H^* \rightleftharpoons \frac{1}{2}H_2(g) + {}^*, \quad (ES8)$$

$$CO^* \rightleftharpoons CO(g) + {}^*. \quad (ES9)$$

If we treat all but steps (ES1)* and (ES7)* as quasi-equilibrated then the overall rate for this process (assuming steady state) can be written out as follows:

$$r_{\text{overall}} = r_1 = r_7 = k_1^+ P_{CH_4}\theta_*^2 - k_1^-\theta_{CH_3}\theta_H = k_7^+\theta_C\theta_O - k_7^-\theta_{CO}\theta_*. \quad (14)$$

From the expressions for the equilibrium constants it is possible to replace θ_{CO}, θ_O, and θ_C at the right side of the equation above:

$$\theta_{CO} = P_{CO}\theta_*/K_9, \quad (15)$$

$$\theta_O = K_2K_3K_8^2P_{H_2O}\theta_*/P_{H_2}, \quad (16)$$

$$\theta_C = K_4K_5K_6K_8^3\theta_{CH_3}/P_{H_2}^{3/2}. \quad (17)$$

At the left side of the expression for the overall reaction rate, θ_H equals:

$$\theta_H = P_{H_2}^{1/2}\theta_*/K_8. \quad (18)$$

θ_{CH_3} can be expressed as a function of θ_*, with all other unknowns (i.e. rate constants and equilibrium constants) being determined from DFT calculations or scaling relationships, as outlined in the methodology section:

$$\theta_{CH_3} = \frac{(A+B)}{(C+D)}\theta_*, \quad (19)$$

where:

$$A = k_1^+P_{CH_4}, \quad (20)$$

$$B = k_7^-\frac{P_{CO}}{K_9}, \quad (21)$$

$$C = k_1^-\frac{P_{H_2}^{1/2}}{K_8}, \quad (22)$$

$$D = K_2K_3K_4K_5K_6^5k_7^+\frac{P_{H_2O}}{P_{H_2}^{5/2}}. \quad (23)$$

By defining the coverage of species i as the product of a ratio (λ_i) and the coverage of empty sites (θ_*) we can now determine θ_*,

$$\theta_* = \frac{1}{1+\sum_i\lambda_i} \quad (24)$$

and consequently the overall rate expression given above. For the discussion we shall use the scaling relationships to determine the total energies and subsequently the rates. The scaling relations

[4] The coverage due to the calculation set up is effectively 0.5 monolayer with respect to the step sites. This corresponds to essentially non-interacting adsorbates, for example lowering the coverage along the step on Ni{211} to 0.25 monolayer has a negligible influence on the adsorption energy.

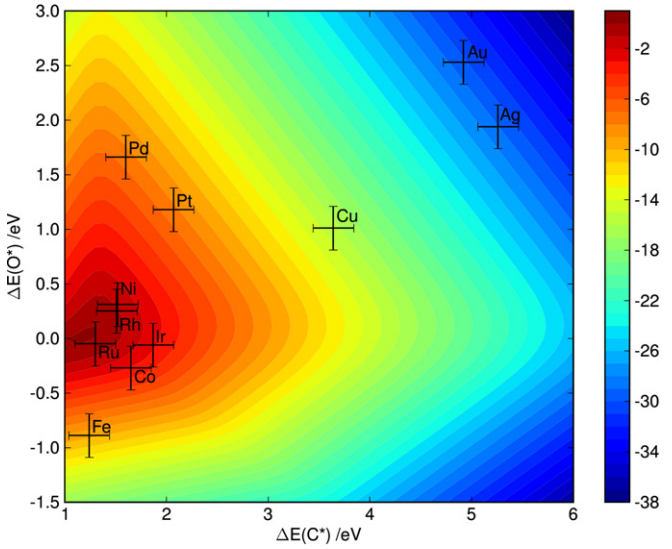

Fig. 6. Two-dimensional volcano-curve of the turn over frequency ($\log_{10}$) as a function of O and C adsorption energy. $T = 773$ K, $P = 1$ bar; 10% conversion. The error bars include an estimated 0.2 eV uncertainties in the adsorption energies.

possess particularly important properties. First of all, they show that to a first approximation only two independent variables, ΔE_C and ΔE_O, characterise the metals. All other adsorption energies and reaction barriers depend linearly upon these underlying variables. Secondly, rather than just calculating rates for discrete points given by the specific elements of the Periodic Table, it is possible to obtain the rate as a function of these two independent variables ($\Delta E_C, \Delta E_O$). This allows us to probe the rate of steam reforming in all of the T, P and adsorption energy phase space. It should be noted that this approach is generally applicable to many processes, where the elementary steps can be described by a scaling relationship. This greatly simplifies the understanding and reveals the trends in reactivity. One particular advantage of the scaling method is that it allows us to probe not only the influence of temperature and pressure on the reaction for each metal, but also permits variation of the adsorption energy of oxygen and carbon and hence rationalise their effect. Fig. 6 depicts the 2D plot comparing the influence of the C and O adsorption energy on the rate at 773 K, 1 bar of pressure having a conversion of 10%. It is seen that the peak of the volcano plot (i.e. where the rate is highest) lies close to the region of the Ni, Rh and Ru adsorption energies, in good agreement with the thermodynamic analysis. The peak lies in the region where the influence of the CO formation and CH_4 adsorption are roughly balanced and that there is competition between these two processes. We do not have a single descriptor as for some reactions, but instead require two descriptors to describe the complete phase space; this was also found to be the case for the water–gas shift reaction [60]. This is as expected from inspection of the BEP relations where the CH_4 dissociation barrier scales with the C adsorption energy, yet both the C and O energy are required to describe the CO formation barrier correctly.

5. Experimental results

The modelling in the previous section gave an estimate of the individual reactivity at a certain set of conditions. In the following experimental results at similar conditions from activity measurements and catalyst characterization are presented. Firstly, the TEM, XRD and sulphur chemisorption results for the average metal particle diameter and metal dispersion are described. Secondly, the structural results are combined with measured activities to deter-

mine the reactivity of methane per surface atom, represented as the turn-over frequency (TOF), for the different metal catalysts.

5.1. TEM measurements

From several TEM images acquired for each sample, the particle size distributions were determined from measurements of more than 400 individual particles. Fig. 7 shows representative *ex situ* TEM images for Rh catalysts in their fresh and aged states. From the particle size distributions, as shown in Fig. 8, the number-averaged particle sizes and dispersions were calculated and are shown in Table 1. A comparison of two individual data sets obtained for a single sample showed a statistical uncertainty (2σ) of 4% in the measurements of the average particle size. The uncertainty due to the microscope magnification calibration was ca. 10%. From these contributions, the absolute uncertainty of the average particle diameter is estimated to be approximately 14%. The TEM images in Fig. 7 and results in Table 1 shows that the fresh samples contained metal particles with an average diameter in the range 1–6 nm and that the particle diameters increased and the dispersion decreased correspondingly with ageing of the different metal catalysts.

It is well-known that Ru is prone to oxidation in the surface [61], and so one may speculate that the passivation procedure affected the Ru particle size so the *ex situ* TEM measurements revealed an incorrect particle size. The fact that the number-averaged particle diameter for the fresh Ru catalyst is about twice as large as for the other metals could reflect such an effect (Table 1). Environmental TEM (ETEM) measurements were therefore conducted to image *in situ* the fresh metal catalysts with 1 wt% metal loading. These catalysts have the smallest particle sizes and so an effect of passivation is expected to be most pronounced for these catalysts. ETEM images of the catalysts are obtained during exposure to 1.2–1.4 mbar of H_2 at 773 K and the analysis for average particle size and dispersion is carried out in the same way as for *ex situ* TEM measurements. Figs. 9a and 9b show representative TEM images of the Ru sample obtained *ex situ* and *in situ* and indicate that a larger fraction of smaller particles were present during in situ observations. The finding is further corroborated by the results presented in Table 1, which reveal that average particle size for the fresh Ru sample (Ru-2) was reduced by a factor of two to 2.1 nm in the ETEM experiment. In comparison, the fresh Rh, Pt, Ni, Pd, and Ir catalysts have also been investigated thoroughly by ETEM. For these catalysts, the results show no difference between the *ex situ* and *in situ* determination of the average particle sizes (Table 1). Since Ru seems to be the only metal affected by passivation, we also investigated the aged Ru catalyst (Ru-2) *in situ* in

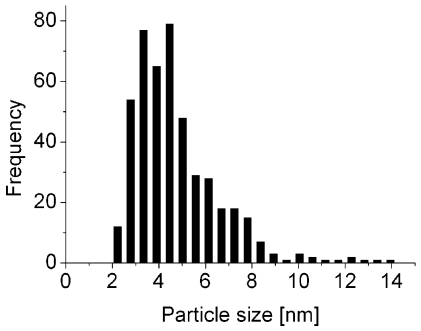

Fig. 8. The particle size distribution of the Rh-3 catalyst with an average particle size of 4.5 nm (i.e. 21% dispersion). A total of 466 particles are included.

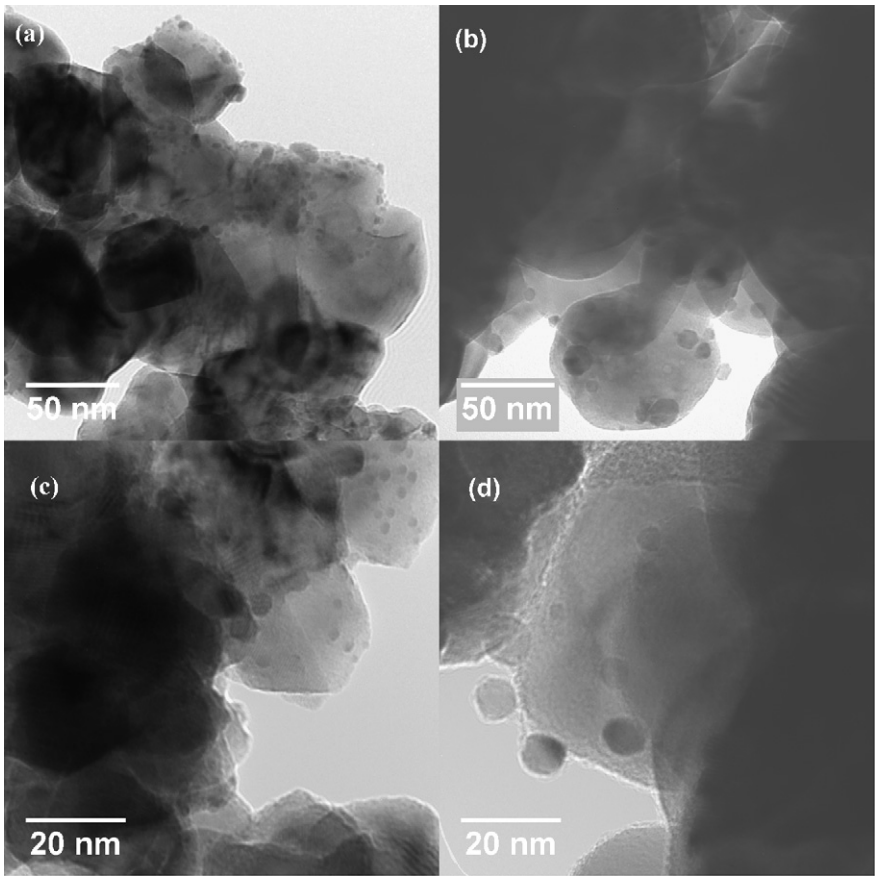

Fig. 7. TEM images of Rh/ZrO_2 catalysts showing the effect of ageing. (a) Fresh 5 wt% Rh-3 and (b) aged 5 wt% Rh-8 (600 h/1096 K) with the average particle diameters of 4.5 and 11.1 nm, respectively. (c) Fresh 1 wt% Rh-1 and (d) aged 1 wt% Rh-2 (228 h/1103 K) with average particle diameters of 2.7 and 8.4 nm, respectively.

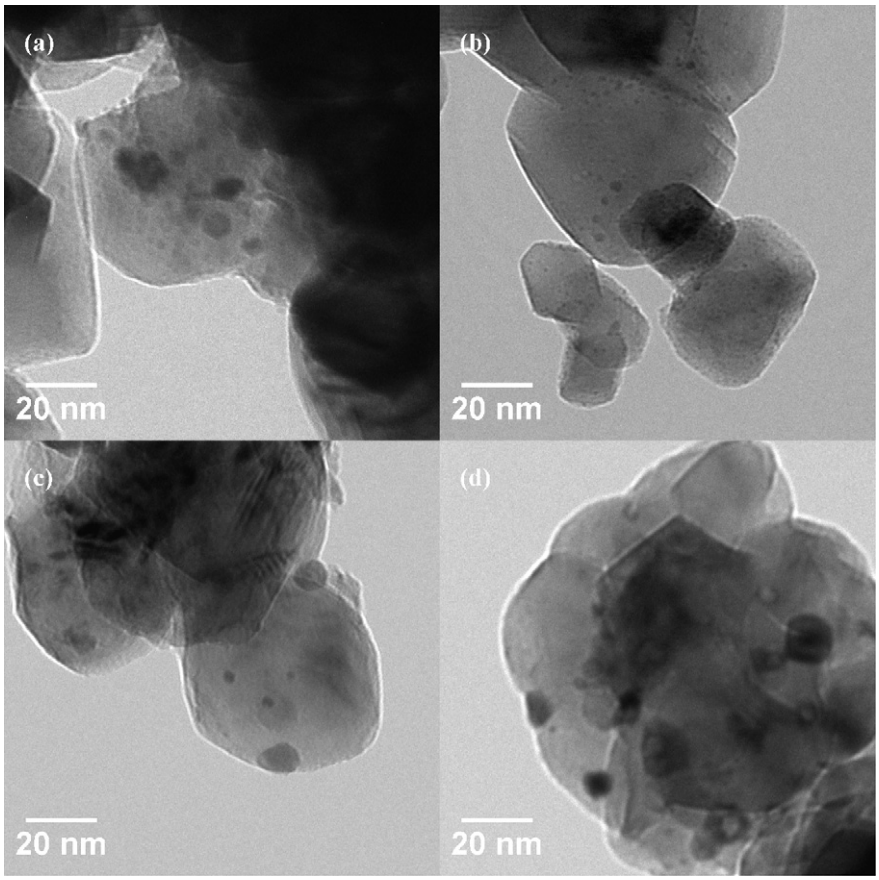

Fig. 9. *Ex situ* and *in situ* microscopy of Ru/ZrO_2. (a) TEM image and (b) ETEM image (1.4 mbar H_2, 773 K) of the fresh Ru catalyst (1 wt% Ru-1). The average particle size was 4.2 nm and 2.1 nm under *ex situ* and *in situ* conditions, respectively. (c) TEM image and (d) ETEM image (1.4 mbar H_2, 773 K) of the aged Ru catalyst (1 wt% Ru-2). The average particle size was 7.2 nm and 7.5 nm under *ex situ* and *in situ* conditions, respectively.

the H_2 environment by ETEM. Figs. 9c and 9d indicate that the Ru particles in the aged catalyst apparently had similar size in the *ex situ* and *in situ* observations and Table 1 further show that the average particle size was large (Ru-2: 7 ± 0.3 nm) and independent of whether the measurements were performed *in situ* or *ex situ*. Hence, the passivation procedure reduced the visibility of 2–4 nm wide Ru particles whereas the effect was less significant for the other metals and larger Ru particles. In order to accurately determine the TOF and dispersion of the fresh ruthenium catalyst, we therefore used the average particle size obtained from *in situ* observations using ETEM. For the other catalysts the particle diameters obtained *ex situ* were used.

5.2. Characterization by sulphur chemisorption and XRD

To confirm the average particle sizes determined by TEM, the 5 wt% Rh catalysts have been characterized by integral methods including sulphur chemisorption and XRD. In Fig. 10 (left) is shown the good correlation between the average diameter obtained by sulphur chemisorption and the surface-averaged diameter obtained by TEM. Fig. 10 (right) shows that the average crystal sizes determined by XRD show the same level as the volume-averaged diameter obtained by TEM. However, the crystallite diameter as obtained by XRD is smaller than actual particle size. The discrepancy could likely be due to twinning of the individual Rh particles (Fig. 11), which causes particles to appear as polycrystals so that the average crystal size becomes smaller than the average particle size. Hence, it is expected that the diameters determined by XRD fall below those obtained by TEM.

5.3. Activity measurements

All catalysts were tested for their activity in steam reforming of methane. The series of Rh catalysts were prepared to obtain a variation in particle sizes so that any structural effect on the activity can be revealed. The remaining Ru, Ir, Pt, Pd and Ni catalysts were tested to allow a ranking of the different metals with respect to their TOF. In the activity measurements, the catalyst amount was adjusted to a conversion of about 10%, and definitely less than 15%. The steam-to-carbon ratio was set to 4. The turnover rates of the catalysts are given in Table 1 and plotted versus dispersion in Fig. 12. For the Rh catalysts, there is a pronounced dependence of the turnover rate on the dispersion; i.e. the turnover number is increasing with higher dispersion and smaller particle sizes. This finding indicates that the activity depends on the detailed surface structure of the nanoparticles and that the low-coordinated surface sites play an important role for the relative activity of the active metals for steam reforming because smaller particles are expected to expose a larger fraction of low-coordinated sites than larger particles [62,63]. It is particularly interesting to note that for Rh, the turnover rate increases nearly linearly with dispersion. Fig. 12 shows that by comparing the different metals at the same dispersion (e.g., 0.4) that the activity is highest for Rh and Ru-based catalysts and is decreasing in the following order: Rh $\sim$ Ru $>$ Ni $\sim$ Ir $\sim$ Pt $\sim$ Pd.

6. General discussion

The 2D volcano plot of the steam reforming rate (Fig. 6) shows the peak activity to be at a slightly lower C adsorption energy than

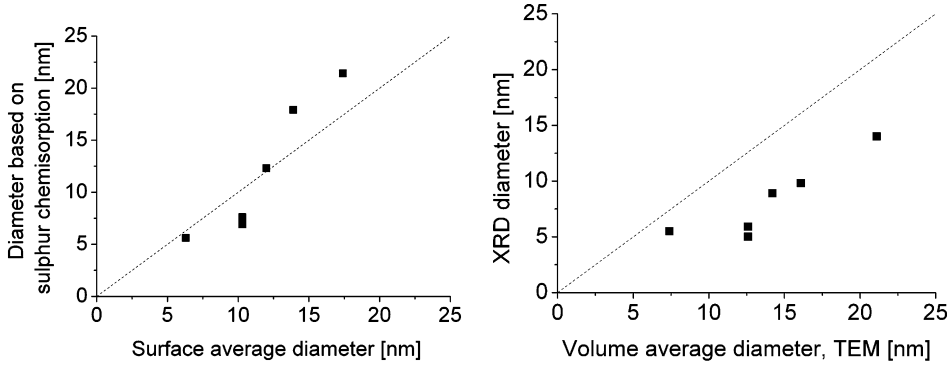

Fig. 10. Diameter by sulphur chemisorption vs. surface average diameter (left). Diameter by XRD vs. volume averaged diameter (right).

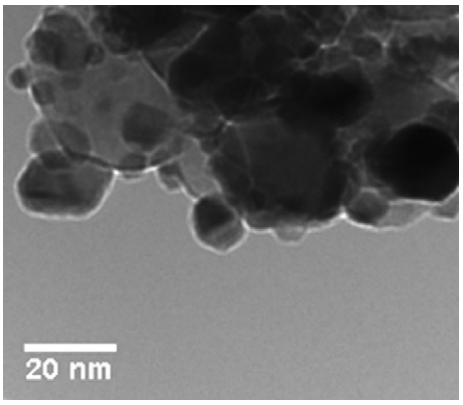

Fig. 11. TEM image of Rh/ZrO_2 (Rh-6) showing twinning plane in a Rh nanoparticle.

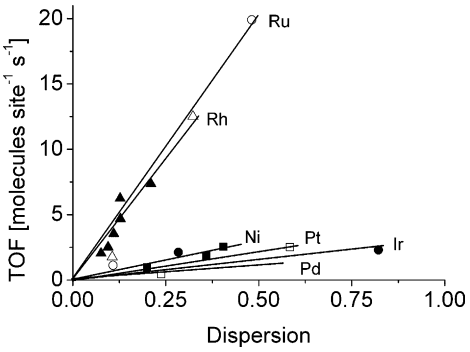

Fig. 12. Reaction rate as a function of dispersion for CH_4–H_2O reforming (773 K, 0.19 bar CH_4, 0.74 bar H_2O, 0.07 bar H_2). Ru (○), 5 wt% Rh (▲), 1 wt% Rh (△), Ni (■), Pt (□), Ir (●) and Pd (◆).

that of the pure metals with the highest activity (Ru, Rh and Ni). If we raise the temperature, the peak of the volcano moves out to even lower C adsorption energies, however, the general reactivity trend is maintained with the activities of Rh, Ni and Ru being almost indistinguishable (see supplementary materials for further information). If we turn our attention to the experimental order of reactivity (Fig. 12) at constant dispersion (e.g., 0.4) we see that Rh and Ru have a comparable and high activity while Ni, Pt, Ir, and Pd have lower and comparable activities at similar dispersions. It should be noted however that the theoretical determined rates drop off considerably faster than those determined experimentally, as one moves towards the more noble metals (see supporting material for more details). This is actually observed for several catalytically interesting systems [64] however up to now the precise reason has remained elusive. An important part of the answer is that the accuracy of calculated rates are considerably smaller away from the maximum where the compensation between different elementary reactions makes the overall rate quite independent of the absolute value of the interaction energies. Away from the maximum the error in an activation energy of the order $2kT$ will show up as an order of magnitude error in the rate. Other possible reasons may well be that the rate becomes so low out in the tail of the volcano that another process is causing the catalytic turnover. This could be a reaction path different from the one prevailing for the most active catalysts or it could be that defects or even impurities start to dominate. In these cases we are no longer measuring the rate due to the metal present. If other processes take over this is a sign that the rates are small anyhow and the calculations still describe the right trends. The important point is that we are able to get reasonable rates close to the maximum (where they are most interesting) and that we can describe the trends as discussed below.

Overall the picture we have is that under the assumption that the support effects are negligible the trend from our experimental work is as follows:

$$\text{Ru} \sim \text{Rh} > \text{Ni} \sim \text{Ir} \sim \text{Pt} \sim \text{Pd}$$

and the following trend from theory:

$$\text{Ru} > \text{Rh} > \text{Ni} > \text{Ir} > \text{Pt} \sim \text{Pd}.$$

Whereas there is not exact agreement the general trends are the same and it must be borne in mind that we have a number of sources of error both in the experiments and in the modelling. For instance, some of the discrepancy in the exact trend might result from the morphology of the nanoparticles under experimental conditions.

From inspection of the slopes in Fig. 12, it can be observed that there is a reasonably linear dependence between the TOF and dispersion. The TOF has been extracted from the experimental data assuming that the process proceeds at all surface sites i.e. $\text{TOF} = r/A$, where r is the rate and A is the surface area. However, this may not be the case since we have seen that the steps and defects are much more reactive due to under-coordination effects. Therefore the rate can be written not as due to atoms sitting at the terraces but due to those sitting at the steps and corners. It would be more correct to write the rate as a sum over these different contributions as follows:

$$r = k_t A_t + k_s A_s + k_c A_c, \tag{25}$$

where the subscript t, s, c referrers to terrace, steps, and corners respectively. This means that the TOF can be written as a sum that scales as:

$$\text{TOF} = r/A \cong k_t + k_s g_s \frac{1}{d} + k_c g_c \frac{1}{d^2} \cong k_t + k_s g_s' D + k_c g_c' D^2, \tag{26}$$

where the geometrical factors (g) are constants since the dispersion, $D = A/V$, where V is the volume, scales as $1/d$ for not too

small particles. The important message here is that if only the terrace atoms are active the TOF would appear constant as a function of dispersion, while if steps are dominant it would increase linearly and if corners are dominant it would increase by the square of the dispersion.

The observed increase in the TOF shown in Fig. 12 clearly indicates that the reactivity is dominated by steps and corners and is in good agreement with theoretical results. A more detailed description like the one found in [57] is not possible at this stage. The morphology may change with chemical gas composition and temperature and thereby also influence the reactivity.

The input energies for the kinetic model are all determined from the same technique (i.e. DFT and scaling relationships), rather than a mixture of experimental techniques and theory, hence we would expect most systematic errors to cancel out. However, there are potential errors we should consider: We expect the DFT adsorption energies to possess errors of approximately 0.2 eV, however, we expect energy differences to be more accurate. The applied scaling relationships show a mean absolute error of 0.14 eV as detailed in reference [49]. These uncertainties must also be considered in the context of the volcano plot, where such errors are not expected to perturb the reactivity trends significantly. Absolute rates may therefore deviate by a few orders of magnitude, but the calculated reactivity trend is not expected to deviate from experiment. This is particularly important when considering the predictive power of the theoretical model.

It is evident that both our theoretical and experimental reactivity trends are in reasonable agreement with Kikuchi et al. [13], Rostrup-Nielsen and Hansen [4,12] and Qin et al. [9]. However, the reactivity trend reported here is significantly different from that obtained by Wei and Iglesia [11], though all metals are within an order of magnitude. The reason for this discrepancy is not known, but we will now proceed to discuss some of the differences between the present experimental work and the work of Wei and Iglesia.

First the experimental conditions will be considered. Wei and Iglesia work at slightly higher temperatures than we do (823–1073 K vs. 773 K). They find the rate-determining step to be methane activation in good agreement with our theoretical work, which shows that the rate-determining step switches from the CO formation step to the methane activation step in this temperature regime in accordance with the previously suggested two-step mechanism. There is general agreement that steam reforming is first order in methane [4], but an overall negative pressure dependency in our previous measurements [4] differs from the results of Wei and Iglesia [11] that showed no impact from other reactants than methane. This may be explained by the different temperatures and pressures involved. Using extrapolation of data for the retarding effect of steam for ethane reforming [19] shows that it becomes negligible above 900 K.

Wei and Iglesia have in some cases used high conversion compared to what was used here, as indicated by their reported approach to equilibrium. We have therefore increased the conversion in our theoretical model to 30% in order to see what influence this may have. This has the effect of moving the peak of the volcano towards the Rh, Ni and Ru points, essentially leaving us with the same trend as we observed at the lower conversion of 10%. This evidence implies that it is not a difference in the conversion that is responsible for the difference in the reactivity trends. Theory also shows that the surface coverages are small at higher temperatures, which also corresponds with the work of Wei and Iglesia who report the same findings experimentally.

Support effects were mentioned in the introduction and it has previously been shown that the support has limited effect on the activity of the individual metals [12,15], provided that the support is alkali-free. Even traces of alkali may have a significant effect on the activity [4,12,19]. The only significant support effect expected here is the variance of metal dispersion on different supports [11]. Since the dispersion was determined here by various methods and very thoroughly by TEM, it is not likely that the reported differences arise from support effects. If neither the temperature, conversion nor the coverage effects account for the difference in the reactivity trends, then we can expand the considerations to the experimental set-up and analysis.

The initial catalyst grain size in this investigation was 300–500 μm. Interestingly, we observed in activity tests with smaller catalyst grains or very fine catalyst powder tabletted with catalytically inert material and crushed again according to the method used by Iglesia and Wei, resulted in a significant loss of activity at 823 K and above. After some time the activity stabilized but at a lower level than the activity obtained for the medium sized particles (300–500 μm). This phenomenon has been tested and observed for reforming catalysts containing Rh, Ru, and Ni. At present it is speculated that support effects are causing this deactivation, possibly a weak metal support interaction as observed for example for Rh on Al_2O_3 [65,66] and ZrO_2 [67]. This phenomenon justified the chosen catalyst particle size in our experiments. The temperature used in this study of 773 K was chosen to get a stable activity and to measure at a temperature where catalyst activity is most important in tubular steam reformers [19]. No quantitative measurements of the decrease in activity have been performed, but qualitatively a difference is observed in the effect on the different metal/support systems. Therefore deactivation of the catalyst to a different extent could change the ranking of the various metals with respect to their reforming activity. We note that if we extrapolate the TOFs measured by Iglesia and Wei to 773 K using their measured activation energy of 91 kJ/mol we estimate a TOF that is approximately 20 times smaller than our corresponding values. In relation to this we will turn to a discussion of measured methane sticking probability.

Iglesia and Wei suggest that there is a large discrepancy between the CH_4 sticking probabilities measured on single crystal Ru(0001) [18] and those extracted from their rate data. From the data of Wei and Iglesia [11] we estimate the CH_4 sticking coefficient as:

$$S(T) = kN_o\sqrt{2\pi m k_B T},$$

where k is the experimental rate constant of the methane dissociation (which under the assumption that the surface is free of adsorbates) is equivalent to the TOF in $s^{-1}\,Pa^{-1}$ and N_o is the area density of the exposed metal atoms on the catalyst at the hcp closed packed surface (e.g., $1.57 \times 10^{19}\,m^{-2}$ for Ru(0001)). This gives a value of 0.13×10^{-6}. The sticking coefficient measurements on single crystals were carried out between 500 K and 700 K [18]. Using the measured activation energy of $E_a = 0.55$ eV for the single crystal experiment, this value has been extrapolated to 873 K to give a sticking coefficient of 19×10^{-6}. As pointed out by Wei and Iglesia this is two orders of magnitude larger than their value. We can use a similar procedure to extract a sticking coefficient from our rate data. In the case of Ru at 873 K we get a value of 3.5×10^{-6}, much closer to the single crystal value. The DFT calculations give a value of 6.3×10^{-6}, but here the very good agreement is fortuitous, given the uncertainty in the calculated activation energy. All the numbers for sticking coefficients and TOF are summarized in Table 2.

We conclude that the CH_4 dissociation rate measured by Wei and Iglesia for methane decomposition over Ru is considerably lower than the one extracted from our catalytic data, which is in reasonable agreement with the single crystal data. Abbott and Harrison [17] suggested that the experimental conditions used during the methane decomposition measurement of the sticking coefficient of CH_4 on ruthenium by Wei and Iglesia [11] will lead to an

Table 2
Sticking coefficients at 873 K and CH_4 turnover rate at 773 K for Ru catalyst

	Sticking coefficient ($\times 10^6$) 873 K	Forward CH_4 turnover rate (s^{-1}) 773 K	Reference
DFT/scaling relations	6.3	0.64	This study
1.0 wt% Ru/ZrO_2	3.51	19.9[a]	This study
3.2 wt% Ru/γ-Al_2O_3	0.13	0.83	[6]
Ru(0001)	19		[18]

[a] 48.1% dispersion, 0.19 bar CH_4, 0.07 bar H_2, 0.74 bar H_2O. Total flow rate 24 Nl/min.

underestimation. At the conditions stated in [11], we calculate an ideal transient to pass through the catalyst bed in about 0.1 sec. The extracted sticking coefficient ($\sim 1.3 \times 10^{-7}$) will then lead to a conversion of methane of 0.33 and a deposition of one third of a monolayer of carbon in 0.1 second neglecting blocking the active sites by carbon. These figures and the challenges in establishing a transient of methane with a raise time of less than 0.1 second illustrate the difficulties in measuring the sticking coefficient of CH_4 at the experiment conditions used by Iglesia and Wei. The data indicate that the sticking coefficients of CH_4 derived by methane decomposition could easily be underestimated and it seems impossible to measure larger sticking coefficients than those reported by Iglesia and Wei. However, we do not think that the problems encountered in the measurements of the sticking of CH_4 by methane decomposition exist in the steam reforming rates measured in [11].

7. Conclusion

Firstly, we have been able to build up a complete picture of the reactivity of pure metal catalysts for steam reforming using recently identified scaling relationships. This has been combined with thermodynamic and kinetic models to get a fundamental insight into the steam reforming process. Experimental work has verified the picture, thereby validating such an approach. The calculations suggest that the rate is a function of two parameters, the O and C adsorption energies, and a volcano is found giving the trends in ranking. The volcano has a broad maximum and most metals considered here and in previous experiments, including Wei and Iglesia's, are found to lie close to the maximum. Considering the relative small difference between different late transition metal, both experiments and theoretical results agree with most of the earlier works that the most active pure metals for the steam reforming reaction are Ru and Rh, while Ni, Ir, Pt, and Pd are a little less active. Neither the detailed ranking nor the absolute activities agree with the recent work of Wei and Iglesia where it was found that Pt is the most active steam reforming metal.

Theoretically we are able to probe a wide range of temperatures and pressures and it is observed that at low temperatures and for the noble metals the CO formation step is kinetically the most important reaction step. However, as the temperature and reactivity of the metal increase i.e. the metal becomes less noble, the most kinetically relevant step switches from being CO formation to dissociative methane adsorption. This offers an explanation for the fact that different studies, carried out under different conditions, find different rate determining steps. For example the work of Wei and Iglesia was carried out between 873 K and 1073 K, which would be the correct conditions to observe methane activation as the rate determining step.

As well as presenting the fundamental picture from the corroboratory views of theory and experiment, we have also seen in this paper how the theoretical scaling relationships can be used. For simple hydrogenated species it has been shown that we can screen through a range of transition metals to determine where the optimal pure metal catalyst lies. Furthermore, by having the adsorption energies of hydrogenated species as a function of only two parameters (our C and O adsorption energies) we can rapidly probe all of the available adsorption energies to see what properties the ideal catalyst should posses. This scheme provides new insight into what direction to move in terms of surface reactivity for designing new and better catalysts.

Acknowledgments

Haldor Topsøe A/S acknowledges the participation of the CTCI Foundation, Taiwan, in establishing the ETEM facility. CINF is funded by the Danish National Research Foundation.

CAMD is funded by the Lundbeck Foundation. This work has been supported by the Danish Research Agency through frame work program #26-04-0047. The Danish Center for Scientific Computing is acknowledged for the provision of high performance computing facilities.

Supporting material

Supplementary material for this article may be found on ScienceDirect, in the online version.

Please visit DOI: 10.1016/j.jcat.2008.08.003.

References

[1] A.J. Ragauskas, C.K. Williams, B.H. Davison, G. Britovsek, J. Cairney, C.A. Eckert, W.J. Frederick Jr., J.P. Hallett, D.J. Leak, C.L. Liotta, J.R. Mielenz, R. Murphy, R. Templer, T. Tschaplinski, Science 311 (2006) 484.
[2] J.R. Rostrup-Nielsen, Science 308 (2005) 1421.
[3] G.W. Huber, J.N. Chheda, C.J. Barrett, J.A. Dumesic, Science 308 (2005) 1446.
[4] J.R. Rostrup-Nielsen, J. Sehested, J.K. Nørskov, Adv. Catal. 47 (2002) 65.
[5] J. Xu, G.F. Froment, AIChE J. 35 (1989) 88.
[6] J.M. Wei, E. Iglesia, J. Phys. Chem. B 108 (2004) 7253.
[7] J.R. Rostrup-Nielsen, J.-H.B. Hansen, J. Catal. 144 (1993) 38.
[8] J.M. Wei, E. Iglesia, J. Catal. 225 (1) (2004) 116.
[9] J.M. Wei, E. Iglesia, Phys. Chem. Chem. Phys. 6 (13) (2004) 3754.
[10] J.M. Wei, E. Iglesia, Angew. Chem. Int. Ed. 43 (2004) 3685.
[11] J.M. Wei, E. Iglesia, J. Phys. Chem. B 108 (13) (2004) 4094.
[12] J.R. Rostrup-Nielsen, J. Catal. 31 (1973) 173.
[13] E. Kikuchi, S. Tanoka, Y. Yamazaki, Y. Morila, Bull. Jpn. Pet. Inst. 16 (2) (1974) 95.
[14] D. Qin, J. Lapszewicz, Catal. Today 21 (1994) 551.
[15] R. Craciun, B. Shereck, R.J. Gorte, Catal. Lett. 51 (3-4) (1998) 149.
[16] J. Wei, E. Iglesia, J. Catal. 224 (2004) 370.
[17] H.L. Abbott, I. Harrison, J. Catal. 254 (2008) 27.
[18] R.C. Egeberg, S. Ullmann, I. Alstrup, C.B. Mullins, I. Chorkendorff, Surface Science 497 (2002) 183.
[19] J.R. Rostrup-Nielsen, in: J.R. Anderson, M. Boudart (Eds.), Catalysis, Science and Technology, vol. 5, Springer-Verlag, Berlin, 1984, chap. 1.
[20] H. Yang, J.L. Whitten, Surf. Sci. 289 (1–2) (1993) 30.
[21] J. Schule, P. Siegbahn, U. Wahlgren, J. Chem. Phys. 89 (1998) 6982.
[22] C.-T. Au, M.-S. Liao, C.-F. Ng, J. Phys. Chem. A 102 (1998) 3959.
[23] C.-T. Au, C.-F. Ng, M.-S. Liao, J. Catal. 185 (1999) 12.
[24] P. Siegbahn, I. Panas, Surf. Sci. 240 (1990) 37.
[25] P. Kratzer, B. Hammer, J.K. Nørskov, Catal. Lett. 40 (3–4) (1996) 131.
[26] H. Burghgraef, A.P.J. Jansen, R.A. van Santen, Surf. Sci. 324 (1995) 345.
[27] R.M. Watwe, H.S. Bengaard, J.R. Rostrup-Nielsen, J.A. Dumesic, J.K. Nørskov, J. Catal. 189 (2000) 16.
[28] I.M. Ciobica, F. Frechard, R.A. van Santen, A.W. Kleyn, J. Hafner, J. Chem. Phys. Lett. 311 (1999) 185.
[29] I.M. Ciobica, F. Frechard, R.A. van Santen, A.W. Kleyn, J. Hafner, J. Phys. Chem. B 104 (2000) 3364.
[30] A. Michaelides, P. Hu, in: M.A.C. Nascimento (Ed.), Theoretical Aspects of Heterogeneous Catalysis, Kluwer, Dordrecht, 2001.
[31] I.M. Ciobica, R.A. van Santen, J. Phys. Chem. B 106 (2002) 6200.
[32] G. Henkelman, H. Jonsson, Phys. Rev. Lett. 86 (4) (2001) 664.
[33] H.S. Bengaard, J.K. Nørskov, J. Sehested, B.S. Clausen, L.P. Nielsen, A.M. Molenbroek, J. Rostrup-Neilsen, J. Catal. 209 (2) (2002) 365.
[34] C.J. Zhang, P. Hu, J. Chem. Phys. 116 (2002) 322.
[35] A.T. Anghel, D.J. Wales, S.J. Jenkins, D.A. King, Phys. Rev. B 71 (11) (2005) 113410.
[36] M.A. Petersen, S.J. Jenkins, D.A. King, J. Phys. Chem. B 108 (2004) 5909.
[37] M.A. Petersen, S.J. Jenkins, D.A. King, J. Phys. Chem. B 108 (2004) 5920.

[38] A. Kokalj, N. Bonini, S. de Gironcoli, C. Sbraccia, G. Fratesi, S. Baroni, J. Am. Chem. Soc. 128 (38) (2006) 12448.
[39] A. Kokalj, N. Bonini, C. Sbraccia, S. de Gironcoli, S. Baroni, J. Am. Chem. Soc. 126 (51) (2004) 16732.
[40] B. Hammer, L.B. Hansen, J.K. Nørskov, Phys. Rev. B 59 (1999) 7413.
[41] H.S. Taylor, Proc. R. Soc. London Ser. A 108 (1925) 105.
[42] T. Zambelli, J. Wintterlin, J. Trost, G. Ertl, Science 273 (1996) 1688.
[43] P. Kratzer, E. Pehlke, M. Scheffler, M.B. Raschke, U. Höfer, Phys. Rev. Lett. 81 (1998) 5596.
[44] S. Dahl, A. Logadottir, R. Egebjerg, J. Larsen, I. Chorkendorff, E. Tørnqvist, J.K. Nørskov, Phys. Rev. Lett. 83 (1999) 1814.
[45] F. Abild-Pedersen, O. Lytken, J. Engbæk, G. Nielsen, I. Chorkendorff, J. Nørskov, Surf. Sci. 590 (2005) 127.
[46] T. Bligaard, J.K. Nørskov, S. Dahl, J. Matthiesen, C.H. Christensen, J. Sehested, J. Catal. 224 (2004) 206.
[47] H.J. Monkhorst, J.D. Pack, Phys. Rev. B 13 (1976) 5188.
[48] D. Vanderbilt, Phys. Rev. B 41 (1990) 7892.
[49] F. Abild-Pedersen, J. Greeley, F. Studt, J. Rossmeisl, T.R. Munter, P.G. Moses, E. Skúlason, T. Bligaard, J.K. Nørskov, Phys. Rev. Lett. 99 (2007) 016105.
[50] G. Jones, T. Bligaard, F. Abild-Pedersen, J.K. Nørskov, J. Phys. Condens. Mater. 20 (2008) 064239.
[51] V. Pallasana, M. Neurock, J. Catal. 191 (2000) 301.
[52] J.K. Nørskov, T. Bligaard, A. Logadottir, S. Bahn, L.B. Hansen, M. Bollinger, H. Bengaard, B. Hammer, Z. Sljivancanin, M. Mavrikakis, Y. Xu, S. Dahl, C.J.H. Jacobsen, J. Catal. 209 (2002) 275.
[53] J.H. Noogle, Physical Chemistry, Little Brown and Co, Boston, 1985.
[54] T. Bligaard, K. Honkala, A. Logadottir, J.K. Nørskov, S. Dahl, C.J.H. Jacobsen, J. Phys. Chem. B 107 (2003) 9325.
[55] J. Sehested, J.A.P. Gelten, S. Helveg, Appl. Catal. 309 (2006) 237.
[56] P.L. Hansen, S. Helveg, A.K. Datye, Adv. Catal. 50 (2006) 77.
[57] M.P. Andersson, F. Abild-Pedersen, I. Remediakis, T. Bligaard, G. Jones, J. Engbaek, O. Lytken, S. Horch, J.H. Nielsen, J. Sehested, J.R. Rostrup-Nielsen, J.K. Nørskov, I. Chorkendorff, J. Catal. 255 (2008) 6.
[58] O.R. Inderwildi, S.J. Jenkins, D.A. King, J. Phys. Chem. C 112 (2008) 1305.
[59] O.R. Inderwildi, S.J. Jenkins, D.A. King, J. Am. Chem. Soc. 129 (2007) 1751.
[60] N. Schumacher, A. Boisen, S. Dahl, A.A. Gokhale, S. Kandoi, L.C. Grabow, J.A. Dumesic, M. Mavrikakis, I. Chorkendorff, J. Catal. 229 (2005) 265.
[61] P.G.J. Koopman, A.P.G. Kieboom, H. van Bekkum, J. Catal. 69 (1981) 172.
[62] C.H. Jacobsen, S. Dahl, P.L. Hansen, E. Toernqvist, H. Topsøe, D.V. Prip, P.B. Møenshaug, I. Chorkendorff, J. Mol. Catal. A Chem. 163 (2000) 19.
[63] K. Honkala, A. Hellman, I.N. Remediakis, A. Logadottir, A. Carlsson, S. Dahl, C.H. Christensen, J.K. Nørskov, Science 307 (2005) 555.
[64] H. Falsig, T. Bligaard, J. Rass-Hansen, A.L. Kustov, C.H. Christense, J.K. Nørskov, Top. Catal. 45 (2007) 117.
[65] J.G. Chen, M.L. Colaianni, P.J. Chen, J.T. Yates Jr., J. Phys. Chem. 94 (1990) 5059.
[66] C. Wong, R.W. McCabe, J. Catal. 119 (1989) 47.
[67] A. Gervasini, F. Morazzoni, D. Strumolo, F. Pinna, G. Strukul, L. Zanderighi, J. Chem. Soc. Faradray Trans. I 82 (1986) 1795.